Scientific Research Publishing

American Journal of Analytical Chemistry, 2023, 14, 305-325
https://www.scirp.org/journal/ajac
ISSN Online: 2156-8278
ISSN Print: 2156-8251

Response Surface Methodology-Based SERS for Determination of Gymnodimine

Siyang Chan[1], Yaoyi Wu[1], Yifan Liu[1], Donghang Yin[2*], Fei Wang[1*]

[1]Department of Chemistry, School of Science, China Pharmaceutical University, Nanjing, China
[2]Department of Life and Health, Nanjing Polytechnic Institute, Nanjing, China
Email: *feiwang@cpu.edu.cn, *cpu2013y@163.com

How to cite this paper: Chan, S.Y., Wu, Y.Y., Liu, Y.F., Yin, D.H. and Wang, F. (2023) Response Surface Methodology-Based SERS for Determination of Gymnodimine. *American Journal of Analytical Chemistry*, **14**, 305-325.
https://doi.org/10.4236/ajac.2023.148017

Received: July 24, 2023
Accepted: August 26, 2023
Published: August 29, 2023

Abstract

Gymnodimine (GYM), a fast-acting marine toxin, is destructive to aquaculture and human health through contaminated shellfish. The current detection methods in GYM have definite drawbacks in operation, such as the demand for delicate instruments and the consumption of time. Therefore, silver colloid was utilized as a surface-enhanced Raman scattering (SERS) desirable substrate for sensitive and rapid detection of GYM in lake and shellfish samples. The theoretical spectrum of GYM is calculated by density functional theory (DFT), and the substrate performance is evaluated by a rhodamine 6 G probe. Under the optimal SERS experimental condition calculated by the response surface methodology, the low limit of detection of 0.105 μM with R^2 of 0.9873 and a broad linearity range of 0.1 - 10 μM was achieved for GYM detection. In addition, the substrate was satisfyingly applied to detect gymnodimine in the lake and shellfish matrix samples with LOD as low as 0.148 μM and 0.170 μM, respectively. These results demonstrated a promising SERS platform for detecting marine toxins in seafood for food safety and pharmaceutical research.

Graphic Abstract

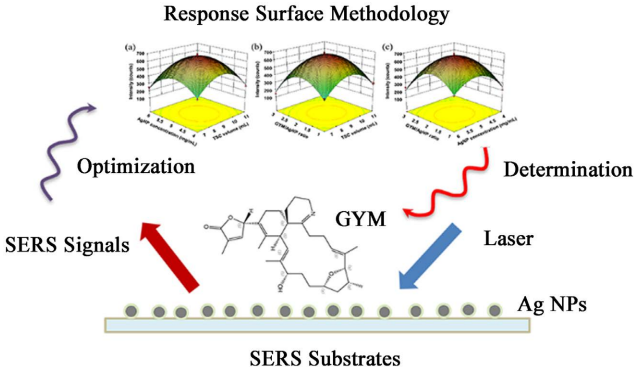

Keywords

Surface-Enhanced Raman Scattering, Gymnodimine, Ag Colloid, Box-Behnken Design, Response Surface Methodology

1. Introduction

Marine toxins in seafood usually accumulate in edible shellfish and fish, causing poisoning symptoms and even life-threatening after human consumption, posing a risk to consumers' health [1]. Shellfish toxins are typically produced by phycotoxins. Since shellfish have a unique way of filter feeding that accumulates pollutants in water, phytoplankton, and even in the ocean, shellfish have become the most common toxin carrier in seafood [2]. Karen algae produced Gymnodimine (GYM), first discovered in New Zealand [3]. This toxin has a specific spiroimide toxic functional group, which is less toxic than other fat-soluble toxins. However, the degradation rate of GYM is prolonged, and thus it has potential long-term harm to eaters [4] [5]. The safety standard of toxin GYM content is currently unclear [6]. Therefore, developing a reliable and sensitive method for GYM detection for food safety is crucial.

At present, the primary detection methods for GYM are mouse bioassay (MBA), liquid chromatography-tandem mass spectrometry (LC-MS/MS), and receptor-binding assay (RBA). MBA is a traditional method for detecting GYM in seafood [3] [7], but this method has low sensitivity, poor specificity, and ethical issues. LC-MS/MS is the most crucial chemical method with high speed, good repeatability, and strong specificity [8]. LC-MS/MS combined with solid phase extraction can detect four lipophilic marine toxins, including GYM, in bivalve shellfish [9]. However, this method requires large precision instruments and sample pretreatment before tedious testing, which limits its application in the actual scene [10] [11]. RBA is to inhibit the specific binding of α-bungarotoxin to nicotinic acetylcholine receptors by GYM. Subsequently, fluorescence and colorimetry are used to detect the specific binding of α-bungarotoxin to nicotinic acetylcholine receptor. However, the specificity of this method is poor [12] [13] [14]. Hence, it is important to develop a simple, rapid, cost-effective and specific "fingerprints" method for gymnodimine analysis.

Surface-enhanced Raman spectroscopy (SERS) observed in 1974 can be applied to work out the critical issues for its advantages, such as signal amplification and high sensitivity [15] [16]. Raman signals can be enhanced by adsorbing samples on the rough surfaces of metal nanostructures, such as gold, silver, copper, and the like [17] [18] [19]. The mechanism of signal enhancement can be divided into two categories: electromagnetic enhancement and chemical enhancement, in which electromagnetic enhancement is the main factor affecting the SERS signal [20] [21]. SERS has been applied to analyze and detect some shellfish toxins to obtain high-precision, rapid, and *in situ* detection. Olson *et al.*

[22] detected the SERS spectra of domoic acid (DA) and saxitoxin(STX) by silver nanoparticle (AgNP) colloids and determined their molecular vibration modes, which proved the feasibility of the SERS technique in the analysis of shellfish poisoning. Subsequently, Huai *et al.* [23] used laser tweezers Raman spectroscopy (LTRS) combined with SERS technology to obtain a detection limit as low as 2 nM in only 2 seconds of integration time. In addition to direct detection, functional group modification on the metal surface can improve the adsorption between metal and analyte, enhancing the Raman signal. Müller *et al.* [24] carried out amination modification on the surface of AgNPs to improve the binding ability and realized the determination of DA in seawater samples with a detection limit as low as 0.416 mM. Cao *et al.* [25] aminated gold nanoparticles (AuNP) and enhanced the capture ability of STX through electrostatic interaction and hydrogen bonds between cysteines. Thus, the dynamic SERS strategy increases the number of hot spots in the substrate, and the detection level of STX reaches 100 nM.

Considering the advantages of SERS technology and the difficulties of natural product synthesis [25] [26] [27], a novel Ag colloid-based SERS method was established for detecting GYM in lake and shellfish matrix samples. In this study, the vibration modes of the GYM are simulated by density functional theory (DFT); the Ag colloids' enhancement factor was calculated using rhodamine R6G as a probe molecule; the Raman intensity was adjusted and optimized by response surface methodology. Finally, the sensitivity and uniformity of the SERS substrate were evaluated. The optimized substrate was subsequently selected for GYM detection at low concentrations in actual samples (lake and shellfish matrix).

2. Materials and Methods

2.1. Chemicals and Instruments

Silver nitrate ($AgNO_3$) was purchased from Sinopharm Chemical Reagent. Trisodium citrate (TSC) was obtained from Shanghai Lingfeng Chemical Reagent. Rhodamine 6G (R6G) was purchased from Aladdin Chemical Reagent. Gymnodimine (GYM) was acquired from National Research Council Canada. All purchased reagents were all analytic grade and directly used without purification. Deionized water was utilized throughout this research.

UV–vis spectra of Ag colloids were obtained by T6 spectrophotometer (General Instrument Co. Ltd., Beijing, China). Shellfish meat homogenate was prepared by Wiggens D130 homogenizer (Germany). Scanning electron microscopy (SEM) (Scios 2 HiVac, FEI) and transmission electron microscopy (TEM) (F20, FEI) are used to characterize the morphology of the SERS substrate. A laser confocal Raman spectrometer (LabRAM HR Evolution, Horiba) coupled with an objective lens (numerical aperture (NA) of 0.75) was employed to obtain SERS spectra, where a 532 nm laser light source and 600 g/mm grating were chosen for measurements.

2.2. Density Functional Theory (DFT) Calculation

All DFT calculations were performed in Gaussian 09 software package. Vibrational mode assignments of the calculated peaks were made by observations of molecular animations in the Gaussview program. In this study, B3LYP method and ef2svp basis set were used to optimize the molecular geometrical structure and simulate the theoretical Raman spectroscopy of gymnodimine. Given solvent effects, all calculations were performed in a methanol environment.

2.3. Preparation of Silver Nanoparticle Colloid

Silver nanoparticle colloids were synthesized by heating silver nitrate solution with trisodium citrate at high temperatures [28]. First, 45 mg silver nitrate was dispersed in 250 mL of deionized water, and heated to boiling in a three-neck flask. Then, 5 mL of 1% trisodium citrate (TSC) solution was immediately added. The mixture was heated for another 1 h to form a silver-gray solution and cooled to room temperature. After being washed and centrifugated 5 times, respectively, the product was redispersed in deionized water and stored in the dark at −4˚C.

2.4. SERS Characterization

Rhodamine R6G was introduced as a Raman probe and prepared at concentrations ranging from 10^{-3} M to 10^{-11} M in deionized water. The stock solution of GYM with 100 μM is diluted with methanol stepwise to prepare analyte concentrations from 10 μM to 0.1 μM. For SERS measurements, 10 μL of AgNP colloids were dropped on the silicon wafer, which was then overlaid with 20 μL of gymnodimine solutions of different concentrations and dried in air. SERS signals were performed on a LabRAM HR Evolution system with a 532 nm laser wavelength, 50 mW of nominal power, and a 50× objective. Signals of 20 regions on the substrate were randomly collected on a silicon wafer to investigate the uniformity of the substrate. The spectra were recorded in the range of 540 - 2000 cm^{-1}, with an acquisition time of 10 s and the accumulation of 2 times. The peak position calibration of Raman spectroscopy was operated on the silicon wafer at 520.7 cm^{-1} before detection.

2.5. The Box-Behnken Design (BBD)

The effect of the individual factors on the GYM detection process was determined by the volume of TSC, the concentration of AgNPs, and the ratio of GYM/AgNPs. Response surface methodology (RSM) was used to evaluate the collective influence of the above three variables and establish a model to optimize the response.

Based on the results of previous single-factor experiments, a three-variable Box-Behnken design (BBD) experiment was designed, considering the volume of TSC (Factor A), the concentration of AgNPs (Factor B), and the bulk ratio of GYM/AgNPs (Factor C). The Design-Expert software 8.0.5b (Stat-Ease, Inc.,

Minneapolis, USA) was used for experiment design and statistical analysis. Table 1 shows the level of factors in the BDD model. According to BBD design, the results of variables on the SERS signal were composed of 17 experiments, which included three repeated measurements of crucial points to eliminate system errors. Data from BBD were fitted to the quadratic polynomial model as equation (1):

$$Y = \beta_0 + \sum \beta_{ii} X_i^2 + \sum \beta_{ij} X_i X_j \quad (1)$$

where Y is the response factor, X_i and X_j are independent variables, and β_i, β_0, β_{ii}, and β_{ij} are the coefficients of linear, constant, quadratic, and cross-product, respectively.

The statistical significance of the BBD model was assessed, and parameters that significantly affected responses were determined by using analysis of variance (ANOVA) and Fisher's statistical test (F-test) at the 95% confidence level (p-value < 0.05). The three-dimensional response surface was presented to explain the influence between variables on the SERS signal of gymnodimine.

2.6. Preparation for the Real Sample Detection

The mussels were purchased from local seafood markets, weighing about 500 g and evenly sized. The water samples were taken from a local lake. 200 mL of lake water was filtered with quantitative filter paper and 0.22 μm microporous membrane to remove impurities, then stored at room temperature for future use. Then, 100 mL of methanol/water (1:1, V/V) was added to the homogenate of shellfish. The solution was ultrasonically treated for 20 min for further extraction and centrifugation. The supernatants were removed from impurities similarly and stored at −4˚C for further use.

The 100 μM of GYM solution was mixed with the above two samples, respectively, to prepare the GYM spiked samples with a concentration range of 0.1 - 10 μM. In the same way, the spectra were recorded by the optimized conditions and SERS analysis procedure.

3. Results and Discussion

3.1. DFT Calculations, SERS Spectra, and Regular Mode Assignments

Figure 1(a) and Figure 1(b) show the molecular structural formula and optimized

Table 1. Independent variables and experimental design levels in the Box-Behnken design.

Independent variables	Coded symbols	Levels		
		−1	0	1
The volume of TSC (mL)	X_1	7	9	11
The concentration of Ag NPs (mg/mL)	X_2	4	5	6
GYM/Ag NPs bulk ratio	X_3	1	2	3

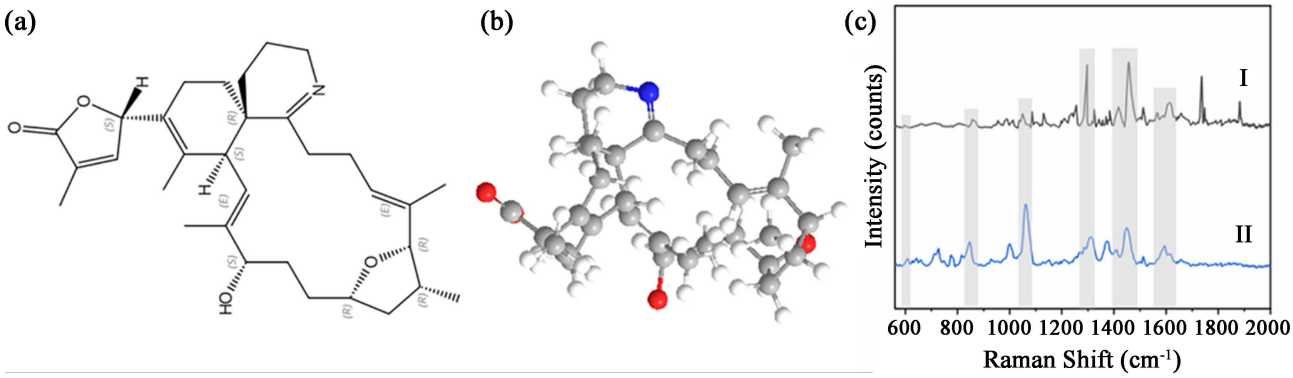

Figure 1. Molecular structure and Raman spectroscopy of gymnodimine. (a) The molecular structural for-mula of gymnodimine. (b) The optimized spatial structural formula of gymnodimine. (c) Peak distribution of gymnodimine theoretical calculation (I) and SERS spectrum (II).

geometries of gymnodimine. As expected, gymnodimine possesses a characteristic cyclic imine structure as a toxic group and oxygen bridge. The calculated DFT spectrum and experimental SERS spectrum of gymnodimine in the 540 - 2000 cm^{-1} range are shown in **Figure 1(c)**, and the peak intensities of the spectra were expressed as normalization approaches, respectively. A good fit of characteristic peak bands between the theoretical calculation and the SERS spectra is obtained, mainly appearing at 620, 820, 1047, 1298, 1416, 1452, and 1735 cm^{-1}. It also indicates the consistency of the predicted RB3LYP/ef2svp method for this molecule.

A detailed assignment of the prominent peaks and vibrational mode of gymnodimine are summarized in **Table S1**. Due to C-C stretching vibration and -OH in-plane bending vibration, an intense band appeared at 1061 cm^{-1}, whereas being given at 1047 cm^{-1} in the DFT calculation. The Raman peaks at 1301 and 1443 cm^{-1} are assigned to out-of-plane and in-plane bending vibration of $-CH_2$, respectively. The bands at 612 cm^{-1} are related to C-C stretching vibration and $-CH_2$ in-plane bending vibration. The stretching vibration of C-O and the in-plane bending vibration of C-C are mainly contributing to the SERS band at 820 cm^{-1}, while the out-of-plane bending vibration of C-H and $-CH_2$ is associated with the bands at 1407 cm^{-1}. However, a DFT theoretical spectrum infers that the band of 1735 cm^{-1} is attributed to the stretching vibration of C=N, which is not observed in the experimental spectrum.

3.2. Selectivity and SERS Activity of the Substrate

Gold, silver, and copper are the most commonly used active substrates [29] in SERS technology. SERS enhancement of the three substrates was studied first. Since the response of the metal surface plasma to the excitation light source wavelength is different, a specific range of laser wavelengths can effectively excite the surface plasmon resonance of the substrate material [30]. Therefore, the 532 nm laser is chosen for signal enhancement. The Raman spectral results are shown in **Figure S1**. Compared with AuNPs and CuNPs, it is evident that the SERS spectrum of AgNPs is most consistent with the DFT theoretical calcula-

tion. Moreover, AgNPs substrate enhances the SERS intensity of the characteristic peaks of gymnodimine. However, AuNPs show shoulder peaks in 1330 - 1530 cm^{-1}, which obscured the relevant characteristic peaks. Meanwhile, for CuNPs, the single Raman peak at 1443 cm^{-1} can be enhanced with significant background noise.

Figure S2 shows the SEM and TEM images of silver colloids. The sliver colloids exhibit uniform quasi-spherical particles with a 60 - 70 nm diameter. The UV-Vis absorption spectra of AgNP colloids are shown in **Figure 4**, and it indicates a clear absorption peak at 422 nm, confirming the formation of AgNPs. The value of full width at half-peak (FWHM) depends on the dispersion of the nanomaterial. The larger the FWHM, the stronger the dispersion of the material is [31]. **Figure S3** also shows a small shoulder around 350 nm, caused by the multilevel transition of the surface plasmon due to the increased size of AgNPs [32].

We have explored the SERS performance of Ag colloids by using rhodamine R6G as a probe molecule. **Figure S4(a)** shows the Raman spectrum and comparative SERS spectra of rhodamine R6G at a concentration of 10^{-6} - 10^{-11} M on silver colloids, and it can be found significant enhancement effect of spectral signal. The characteristic peaks of R6G at 612, 722, 1183, 1361, 1510, and 1650 cm^{-1} are demonstrated, respectively, similar to the literature data [33]. The SERS spectra show that R6G solution can be detected at concentrations as low as 10^{-11} M. The equation for calculating the Raman enhancement factor (EF) of the substrate material according to the method of McFarland *et al.* as Equation (2) [30]:

$$EF = \frac{I_{SERS}/N_{Surf}}{I_{RS}/N_{Vol}} \tag{2}$$

where I_{RS} and I_{SERS} are the normal Raman signal intensity of the rhodamine R6G solution and the SERS signal intensity at the lowest detectable concentration on the silver colloidal substrate. N_{Surf} and N_{Vol} are the average number of molecules detected on R6G solutions with or without SERS substrate materials. The EF calculation results of the silver colloidal base at each characteristic peak of R6G are shown in **Figure S4(b)**. The EF values of R6G at 1510 and 1650 cm^{-1} are measured to be 1.23×10^8 and 1.17×10^8, respectively, which are greater than the value of others.

3.3. Level of the Single Factor

The electromagnetic enhancement mechanism is closely related to experimental factors on the SERS signal intensity [34] [35] [36]. Thus, three factors, including the amount of trisodium citrate, the concentration of AgNPs, or the bulk ratio of AgNPs/GYM, are changed to achieve a superior signal response. The amount of reducing agent can lead to different sizes, although the mechanism of Raman signal enhancement is not unified [37]. As shown in **Figure 2**, TSC amount affects the SERS signal response on GYM, and the best enhancement effect is achieved at 9 ml TSC set. Considering the TSC influence, 7, 9, and 11 mL of TSC

were used as three levels in the BBD model. In addition, the AgNPs concentration effect was investigated in Figure 3. The SERS response for gymnodimine improved when the concentration increased from 2 to 5 mg/mL, due to the extended hot spot areas [38]. However, the SERS signal declined when the concentration exceeded 5 mg/mL, probably explained by lower adsorption of the analyte or the obstruction of excitation light irradiation according to the AgNps aggregation at higher concentrations [39]. Thus, the concentration of AgNPs with ranges from 4 to 6 mg/mL can be considered as three levels in the BBD model.

Figure 4 shows SERS spectra and signal intensity of gymnodimine based on AgNPs/GYM bulk ratio. The characteristic peaks of GYM began to appear when the ratio was 1:4, but the low efficiency of the laser through GYM molecules

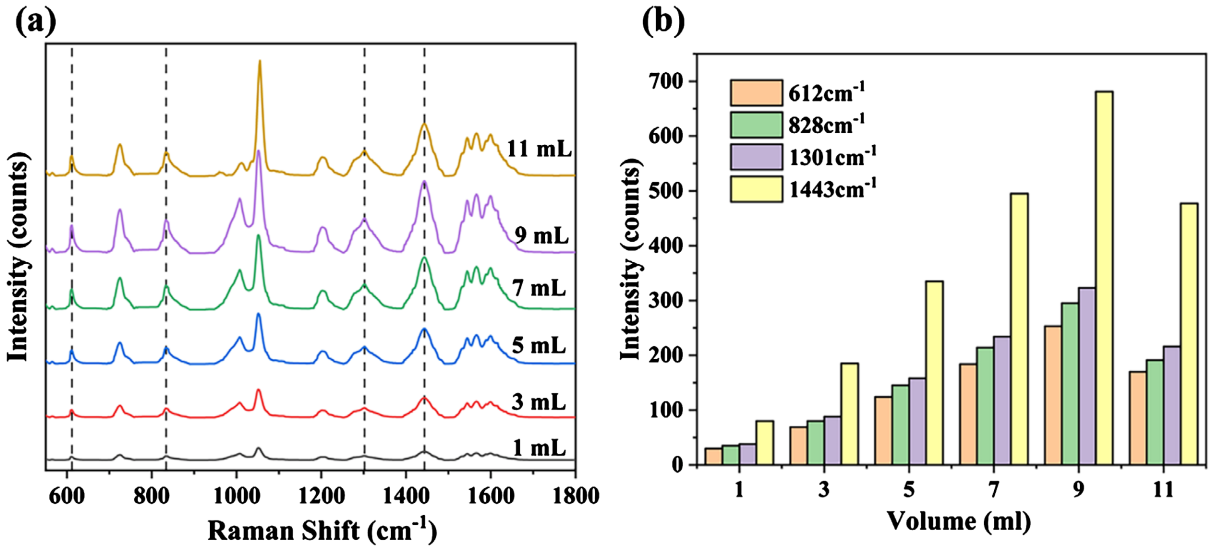

Figure 2. (a) SERS spectra of gymnodimine and (b) Comparison of signal intensity at characteristic peaks of gymnodimine based on AgNPs synthesized with different volumes of TSC.

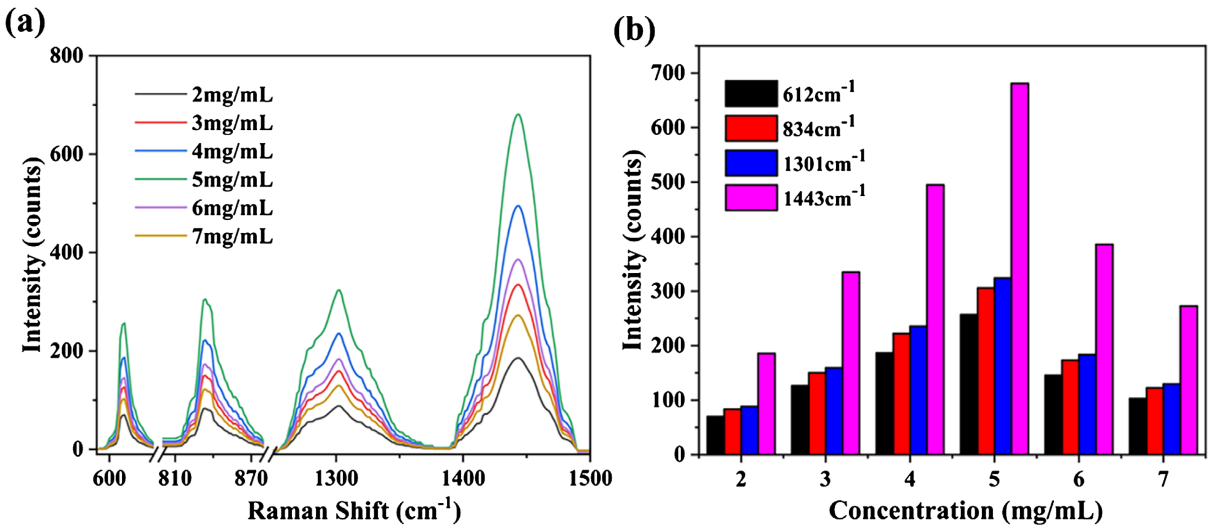

Figure 3. (a) Four characteristic peaks of gymnodimine and (b) Comparison of signal intensity at character-istic peaks of gymnodimine based on different concentrations of AgNPs.

induced surface plasmon resonance in AgNPs caused by the low ratio, which resulted in a minor enhancement of GYM. With the increase of the AgNPs/GYM bulk ratio, the number and the signal intensity of characteristic peaks also increased gradually. However, the SERS signal becomes ambiguous as the ratio increases, which probably generated characteristic peaks about methanol solvent, residual reducing agent, or AgNPs substrate. Thus, only the suitable ratio could better reflect the SERS spectrum of low-concentration gymnodimine [40], and the AgNPs/GYM bulk ratio was regarded as a meaningful variate in the BBD model.

3.4. Optimization of SERS Test

Based on BBD from RSM, 17 experiments were designed and done to optimize the Raman tests further. The coding levels of the solitary factors used in the experimental design and results are shown in **Table S2**. Design-expert 8.05b software was used to perform quadratic regression analysis on the data, and the quadratic polynomial regression equation was shown as Equation (3):

$$\begin{aligned} Y_1 = {} & 673.40 - 16.50X_1 + 41.12X_2 - 63.13X_3 + 5.75X_1X_2 - 5.25X_1X_3 \\ & - 16.50X_2X_3 - 220.45X_1^2 - 190.70X_2^2 - 242.20X_3^2 \end{aligned} \quad (3)$$

where Y_1 was the Raman intensity of GYM at 1443 cm^{-1}, and X_1, X_2, and X_3 were the volume of TSC, the concentration of AgNPs, and the GYM/Ag NPs bulk ratio, respectively.

The results of ANOVA revealed that the experimental data were suitable for the quadratic models (**Table 2**). The p-value was employed to evaluate the significance of each coefficient and indicate the interaction pattern between variables. For GYM, X_2, X_3, X_1^2, X_2^2 and X_3^2 were significantly ($p < 0.05$), while X_1, X_1X_2, X_1X_3 and X_2X_3 were not ($p > 0.05$). The one-way ANOVA and Duncan's multiple range tests indicated that the models were highly significant ($p < 0.0001$) with high F values (82.21). The coefficient (R^2) value of the regression analysis for GYM was 0.9906, which revealed that the model was significant for accurate response prediction, and the adjusted coefficient (Adj $R^2 = 0.9716$) was also a positive value to certify the significance of the model. Therefore, it inferred that the proposed model was appropriate for analyzing the response tendencies.

Regarding the effects of linear and interactive factors, three-dimensional response surface plots (**Figure 5**) were established. While keeping other variables at optimal levels, the response (Intensity) was plotted on the Z-axis for either of the two independent variables. For GYM, the experimental data determined the following optimum operating parameters: volume of TSC of 10.32 mL, concentration of Ag NPs of 5.34 mg/mL, and GYM/Ag NPs ratio of 1.17. Triple parallel experiments were conducted to show that the intensity of the GYM was 687 (relative standard deviation of 3.41%), which was consistent with the predicted value. These results confirmed that the response model sufficiently reflected the expected optimization.

3.5. Sensitivity and Uniformity of SERS Substrate

Gymnodimine is a cyclic imine marine toxin, which is of increasing concern because of its low content and long-term toxicity in living organisms. Since gymnodimine is trace and challengable to extract [41], it is vital to establish an accurate and rapid method for determining GYM. SERS has been proven to be a prospective tool to realize this goal. To study the sensitivity of SERS substrate material, a volume of 10 μL of gymnodimine methanol solution was mixed with

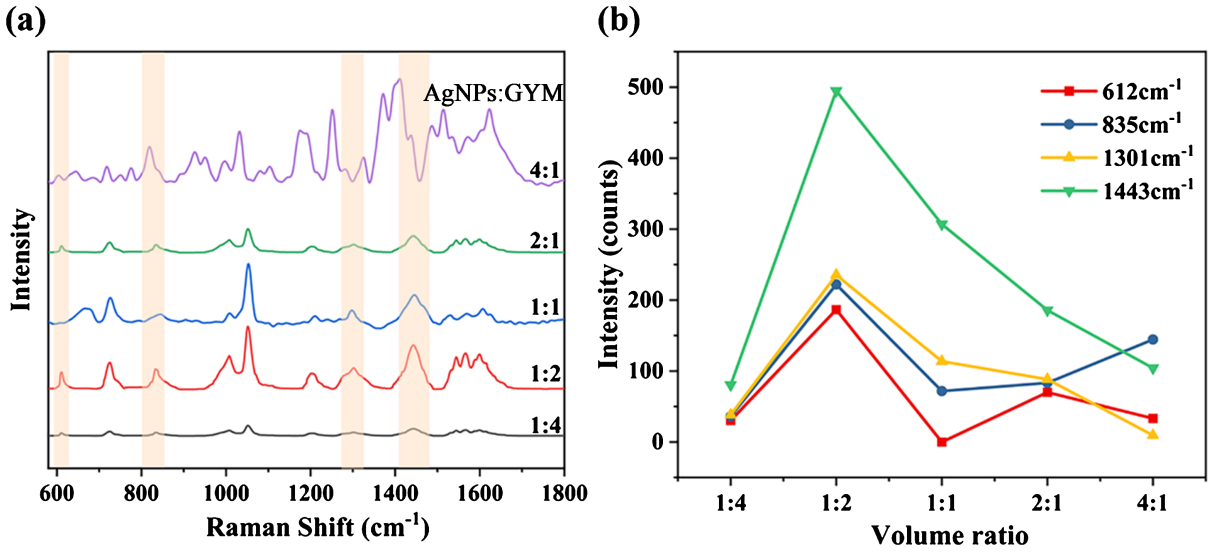

Figure 4. (a) SERS spectra of gymnodimine and (b) Comparison of signal intensity at characteristic peaks of gymnodimine based on different bulk ratios of AgNPs and gymnodimine.

Table 2. Variance analysis for the developed regression model of GYM.

Source	Sum of square	df	Mean squares	F-Value	*p*-Value ($p > F$)
Model	7.24×10^5	9	80,428.78	82.21	<0.0001*
A	2178	1	2178	2.23	0.1793^{NS}
B	13,530.13	1	13,530.13	13.83	0.0075*
C	31,878.13	1	31,878.13	32.59	0.0007*
AB	132.25	1	132.25	0.14	0.7240^{NS}
AC	110.25	1	110.25	0.11	0.7469^{NS}
BC	1089	1	1089	1.11	0.3264^{NS}
A^2	2.05×10^5	1	2.05×10^5	209.17	<0.0001*
B^2	1.53×10^5	1	1.53×10^5	156.52	<0.0001*
C^2	2.47×10^5	1	2.47×10^5	252.48	<0.0001*
Residual	6847.95	7	978.28		
Lack of Fit	5830.75	3	1943.58	7.64	0.0393*
Pure Error	1017.20	4	254.30		
Cor Total	7.31×10^5	16			

*Significant, ^{NS}not significant.

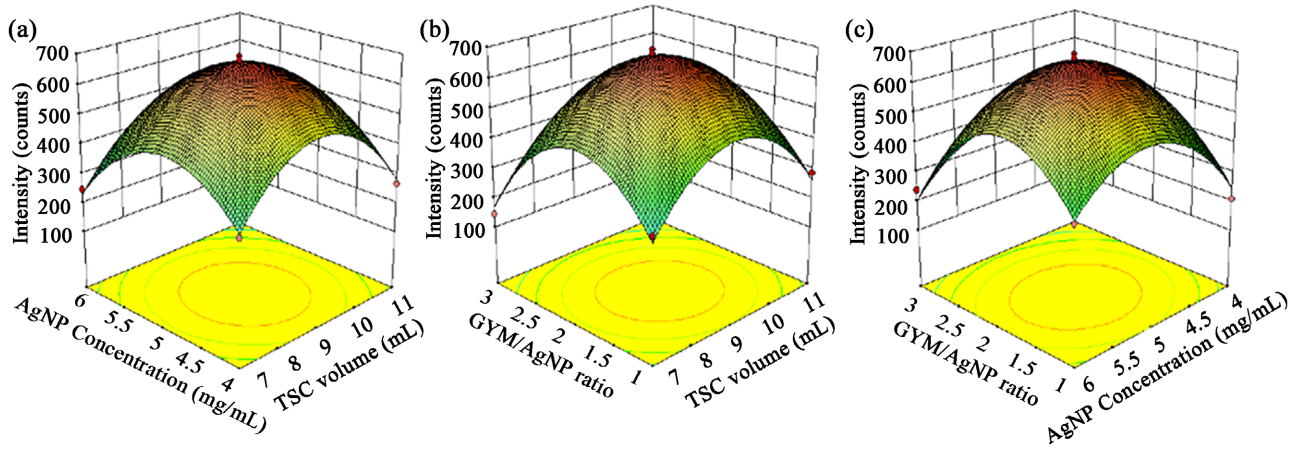

Figure 5. Response surface representations for the detection of the characteristic peak intensity of gym-nodimine under different conditions:(a) The amount of reducing agent and the concentration of Ag NPs; (b) The amount of reducing agent and the volume ratio of the toxins to Ag NPs; (c) The con-centration of Ag NPs and the volume ratio of the GYM to Ag NPs.

AgNPs colloidal solution on the Si wafer for Raman measurement. SERS spectra of different concentrations (10, 8, 6, 4, 2, 1, and 0.1 μM) are collected for detection quantitatively.

Figure 6(a) illustrates the SERS signal of prominent peaks with different concentrations of gymnodimine. As the concentration decreases, the intensity of two characteristic peaks located at 1301 cm^{-1} and 1443 cm^{-1} decreases simultaneously, suggesting a positive cooperation between GYM concentration and peak intensity (Figure 6(a) and Figure 6(b)). Thus, the spectral intensity can be used to quantify GYM in a methanol solution. Table S3 shows the linear relationship and goodness of fit (R^2) in different matrices regarding the intensity of different characteristic peaks versus GYM concentration. Notably, the most excellent fitting equation based on peak intensity at 1443 cm^{-1} in Figure 6(b) is y = 86.224x + 46.771 (where y is SERS intensity, x is GYM concentration) with R^2 of 0.9873. Compared with the blank signal, characteristic peaks of GYM based on AgNPs colloidal can still be observed clearly in a level of as low as 0.1 μM, revealing an efficient sensitivity of SERS substrate. In addition, the limit of detection (LOD) value of GYM in methanol solution was calculated as 0.085 μM and 0.105 μM at 1301 and 1443 cm^{-1} according to the equation of LOD = 3 δ/k [42] [43]. In the formula, δ stands for the standard deviation of spectral intensity of AgNPs colloidal substrates at 1301 and 1443 cm^{-1}, and k represents the slope of the traced calibration curve. The above results prove that the detection of shellfish toxin GYM is feasible on prepared AgNPs colloidal substrate.

It is renowned that the reproducibility of SERS signals is also of great importance that ought to be concerned to demonstrate the prepared nanomaterial as an outstanding SERS substrate [44]. To investigate the reproducibility of GYM based on AgNPs active-substrate, a set of twenty SERS spectra of GYM molecules from different areas on a silicon wafer is acquired under the same experimental conditions as shown in Figure 6(c). The characteristic peak bands collected at different random areas have slight variations in the intensity of Raman

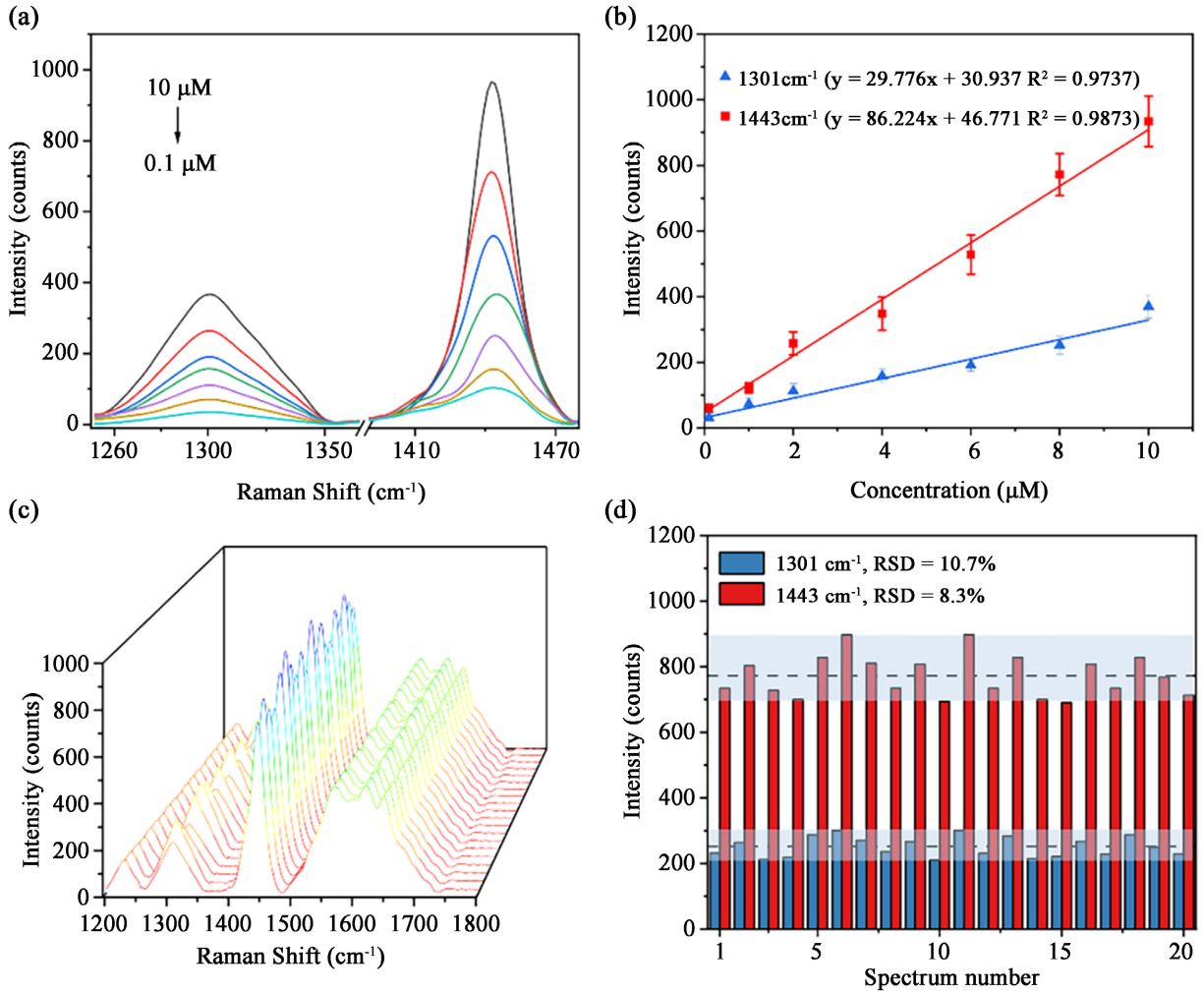

Figure 6. Sensitivity and reproducibility of AgNPs substrate in the determination of gymnodimine. (a) SERS spectra of gymnodimine concentration from 0.1 μM to 10 μM; (b) The Linear relation between Raman characteristic peak intensity and GYM concentration; (c) The SERS spectra of gymnodimine and (d) Peak intensity of 1301 cm^{-1} and 1443 cm^{-1} at 20 sampling sites on the AgNPs substrate.

spectra and no significant change in position, indicating that AgNPs colloidal as the SERS substrate displays well reproducibility. The corresponding intensity and relative standard deviation (RSD) of correlative characteristic peaks at 1301 and 1443 cm^{-1} are verified in **Figure 6(d)**. Generally, RSD values controlled to be less than 20% are regarded as encouraging results [45]. The calculated RSD values of 10.7% and 8.3%, respectively reveal the excellent performance and feasibility in real sample detection as a suitable substrate.

3.6. SERS Detection of Gymnodimine in a Real Lake and Shellfish Samples

To further illustrate the practicability of the AgNPs colloidal substrate, the GYM spiked to the lake and shellfish matrix were detected, respectively. As shown in **Figure S5**, the SERS signal of GYM in real samples was recorded to compare with that of methanol solutions and AgNPs colloidal. As labeled, six typical Ra-

man peaks are enhanced in terms of standard GYM solution at 612, 834, 1061, 1301, 1407, and 1443 cm^{-1}. However, characteristic peaks of real samples at 612, 1061, and 1407 cm^{-1} overlapped with that of methanol solutions. Similarly, the Raman peak at 834 cm^{-1} corresponds to that of the proposed substrate. Therefore, characteristic peaks of standard GYM solution at 1301 and 1443 cm^{-1} were extracted for the quantitative analysis of GYM residues in real samples, which were shifted to 1310 and 1447 cm^{-1} in the lake sample, while 1295 and 1445 cm^{-1} in the shellfish matrix, as specific "fingerprint-like" peaks. It is worth noting that the position of characteristic peaks was changed, probably attributed to the competitive adsorption of unknowns in complex samples with the target molecules and the obscuration of the original signal by clutter peaks. Figure 7(a) recorded the SERS spectra of the GYM with different concentrations in treated lake samples. With the increase of GYM concentration from 0.1 to 10 μM, the related characteristic peaks intensity enhanced. The linear relationship of SERS

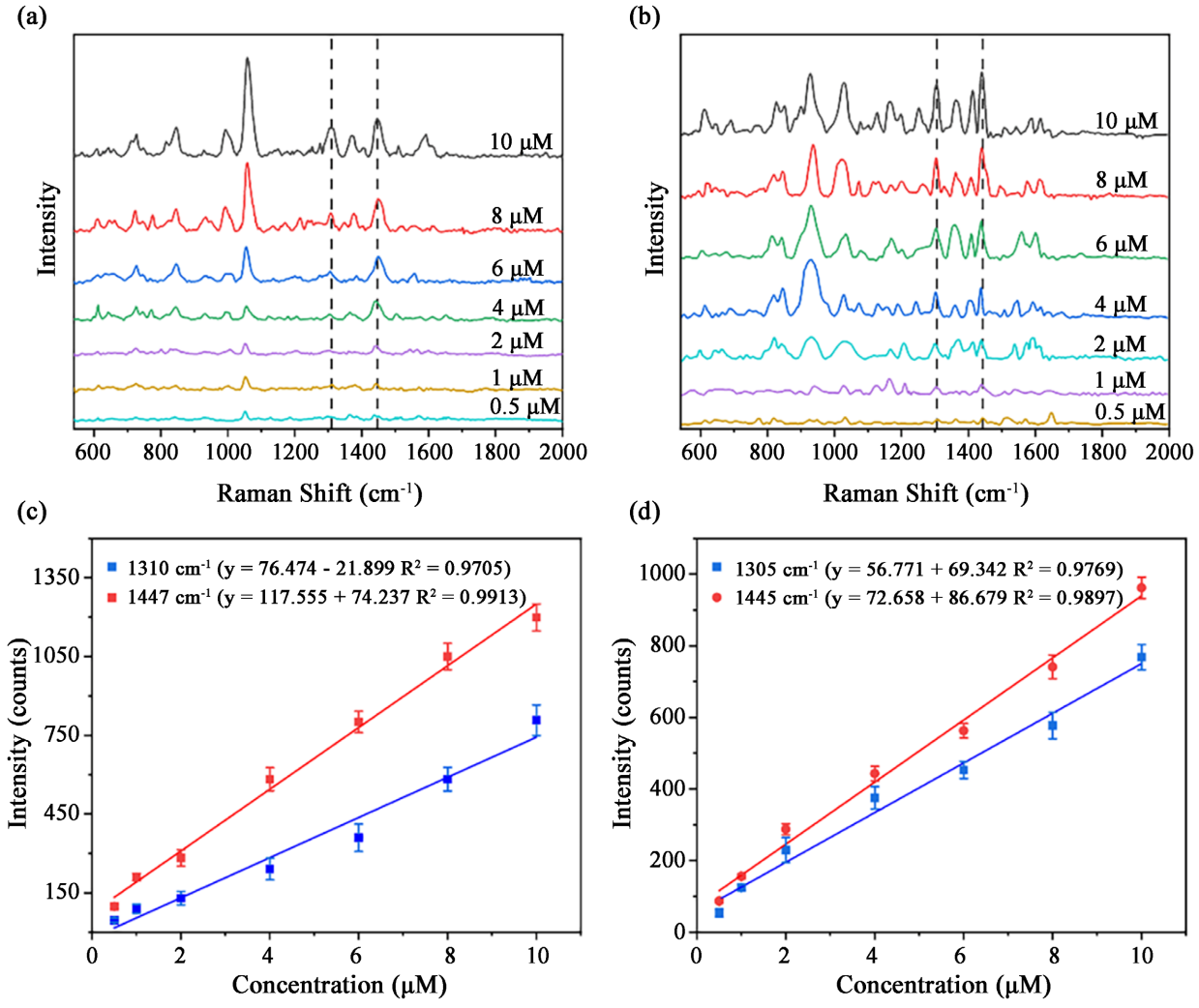

Figure 7. The detection of GYM in lake samples and shellfish matrix samples by SERS. The SERS spectra of GYM in (a) lake and (b) shellfish samples with different concentrations (0.5 - 10 μM); calibration curves at 1310 and 1447 cm-1 with the concentration of GYM in (c) lake and (d) shellfish samples.

intensity at 1310 and 1447 cm^{-1} with the concentration of GYM is illustrated in Figure 7(c). The superior calibration curve at 1447 cm^{-1} was y= 117.555x + 74.237 with R^2 of 0.9913, while the LOD value was measured to be 0.148 μM.

In the same way, the detection of GYM with different concentrations in the treated shellfish matrix, as shown in Figure 7(b), exhibited a reduction in relevant peak intensity with the decrease of GYM concentration. Figure 7(d) shows the linear formula of shellfish matrix samples based on the 1295 and 1445 cm^{-1} bands. The preferable formula at 1445 cm^{-1} was y= 72.658x + 86.679, R^2 was 0.9897, and the LOD value was calculated to be 0.170 μM. The recovery experiment in Table S4 demonstrates that Ag colloid based SERS is suitable for gymnodimine detection in the lake and shellfish matrix samples.

4. Conclusion

This study established a sensitive and rapid method for detecting gymnodimine toxin residues. The vibrational spectrum, theoretical wavenumber, and molecular structure of the GYM were experimentally characterized based on DFT calculation. The highest SERS response was observed by optimizing the volume of TSC, the concentration of AgNPs, and the bulk ratio of GYM/AgNPs by response surface methodology. Ag colloid has an excellent Raman signal response, which supports the desirable sensitivity and uniformity of the SERS substrate. This substrate showed strong SERS performance on the quantitative detection of GYM with LOD of 0.085 μM and 0.105 μM at 1301 and 1443 cm^{-1}, repectively, and with a wide linear range from 0.1 μM to 10 μM. More importantly, the Ag colloid substrate facilitated rapid and accurate detection of GYM residues in the lake and shellfish matrix with the LOD of 0.148 μM and 0.170 μM, which revealed the excellent potential in detecting other shellfish toxins in food analysis and pharmaceutical reasearch.

Acknowledgements

We acknowledge the Cell and Biomolecule Recognition Research Center in China Pharmaceutical University for their technical support.

Conflicts of Interest

The authors declare no conflicts of interest regarding the publication of this paper.

References

[1] Vilariño, N., Louzao, M.C., Vieytes, M.R. and Botana, L.M. (2010) Biological Methods for Marine Toxin Detection. *Analytical and Bioanalytical Chemistry*, **397**, 1673-1681. https://doi.org/10.1007/s00216-010-3782-9

[2] Lopes, V., Costa, P. and Rosa, R. (2019) Effects of Harmful Algal Bloom Toxins on marine Organisms. In: Duarte, B. and Violante Caçador, M.I., Eds., *Ecotoxicology of Marine Organisms*, CRC Press, Boca Raton, 42-88. https://doi.org/10.1201/b22000-4

[3] Munday, R., Towers, N.R., Mackenzie, L., Beuzenberg, V., Holland, P.T. and Miles, C.O. (2004) Acute Toxicity of Gymnodimine to Mice. *Toxicon*, **44**, 173-178. https://doi.org/10.1016/j.toxicon.2004.05.017

[4] Otero, A., Chapela, M.J., Atanassova, M., Vieites, J.M. and Cabado, A.G. (2011) Cyclic Imines: Chemistry and Mechanism of Action: A Review. *Chemical Research in Toxicology*, **24**, 1817-1829. https://doi.org/10.1021/tx200182m

[5] Stewart, M., Blunt, J.W., Munro, M.H., Robinson, W.T. and Hannah, D.J. (1997) The Absolute Stereochemistry of the New Zealand Shellfish Toxin Gymnodimine. *Tetrahedron Letters*, **38**, 4889-4890. https://doi.org/10.1016/S0040-4039(97)01050-2

[6] Toyofuku, H. (2006) Joint FAO/WHO/IOC Activities to Provide Scientific Advice on Marine Biotoxins (Research Report). *Marine Pollution Bulletin*, **52**, 1735-1745. https://doi.org/10.1016/j.marpolbul.2006.07.007

[7] Kharrat, R., Servent, D., Girard, E., Ouanounou, G., Amar, M., Marrouchi, R., Benoit, E. and Molgo, J. (2008) The Marine Phycotoxin Gymnodimine Targets Muscular and Neuronal Nicotinic Acetylcholine Receptor Subtypes with High Affinity. *Journal of Neurochemistry*, **107**, 883-1168. https://doi.org/10.1111/j.1471-4159.2008.05677.x

[8] Chatzianastasiou, M., Katikou, P., Zacharaki, T., Papazachariou, A. and McKevitt, A. (2011) Cyclic Imines, as Emerging Marine Toxins: Chemical Properties, Distribution, Toxicological Aspects and Detection Methods. *Journal of the Hellenic Veterinary Medical Society*, **62**, 240-248. https://doi.org/10.12681/jhvms.14856

[9] Fang, L., Yao, X., Wang, L. and Li, J. (2015) Solid-Phase Extraction-Based Ultra-Sensitive Detection of Four Lipophilic Marine Biotoxins in Bivalves by High-Performance Liquid Chromatography-Tandem Mass Spectrometry. *Journal of Chromatographic Science*, **53**, 373-379. https://doi.org/10.1093/chromsci/bmu054

[10] Liu, Y., Yu, R.C., Kong, F.Z., Li, C., Dai, L., Chen, Z.F. and Zhou, M.J. (2017) Lipophilic Marine Toxins Discovered in the Bohai Sea Using High Performance Liquid Chromatography Coupled with Tandem Mass Spectrometry. *Chemosphere*, **183**, 380-388. https://doi.org/10.1016/j.chemosphere.2017.05.073

[11] Rodríguez, I., Vieytes, M.R. and Alfonso, A. (2017) Analytical Challenges for Regulated Marine Toxins. Detection Methods. *Current Opinion in Food Science*, **18**, 29-36. https://doi.org/10.1016/j.cofs.2017.10.008

[12] Rodriguez, L.P., Vilarino, N., Molgo, J., Araoz, R., Antelo, A., Vieytes, M.R. and Botana, L.M. (2011) Solid-Phase Receptor-Based Assay for the Detection of Cyclic Imines by Chemiluminescence, Fluorescence, or Colorimetry. *Analytical Chemistry*, **83**, 5857-5863. https://doi.org/10.1021/ac200423s

[13] Rodriguez, L.P., Vilarino, N., Molgo, J., Araoz, R., Carmen Louzao, M., Taylor, P., Talley, T. and Botana, L.M. (2013) Development of a Solid-Phase Receptor-Based Assay for the Detection of Cyclic Imines Using a Microsphere-Flow Cytometry System. *Analytical Chemistry*, **85**, 2340-2347. https://doi.org/10.1021/ac3033432

[14] Vilarino, N., Fonfria, E.S., Molgo, J., Araoz, R. and Botana, L.M. (2009) Detection of Gymnodimine-A and 13-Desmethyl C Spirolide Phycotoxins by Fluorescence Polarization. *Analytical Chemistry*, **81**, 2708-2714. https://doi.org/10.1021/ac900144r

[15] Fleischmann, M., Hendra, P.J. and McQuillan, A.J. (1974) Raman Spectra of Pyridine Adsorbed at a Silver Electrode. *Chemical Physics Letters*, **26**, 163-166. https://doi.org/10.1016/0009-2614(74)85388-1

[16] Zhang, D., Liang, P., Chen, W.W., Tang, Z.X., Li, C., Xiao, K.Y., Jin, S.Z., Ni, D.J. and Yu, Z. (2021) Rapid Field Trace Detection of Pesticide Residue in Food Based on Surface-Enhanced Raman Spectroscopy. *Microchimica Acta*, **188**, Article No.

370. https://doi.org/10.1007/s00604-021-05025-3

[17] Tong, Q., Wang, W.J., Fan, Y.N. and Dong, L. (2018) Recent Progressive Preparations and Applications of Silver-Based SERS Substrates. *TrAC Trends in Analytical Chemistry*, **106**, 246-258. https://doi.org/10.1016/j.trac.2018.06.018

[18] Lopez-Lorente, A.I. (2021) Recent Developments on Gold Nanostructures for Surface Enhanced Raman Spectroscopy: Particle Shape, Substrates and Analytical Applications. A review. *Analytica Chimica Acta*, **1168**, Article ID: 338474. https://doi.org/10.1016/j.aca.2021.338474

[19] Markin, A.V., Markina, N.E., Popp, J. and Cialla-May, D. (2018) Copper Nanostructures for Chemical Analysis Using Surface-Enhanced Raman Spectroscopy. *TrAC Trends in Analytical Chemistry*, **108**, 247-259. https://doi.org/10.1016/j.trac.2018.09.004

[20] Ding, S.Y., Yi, J., Li, J.F., Ren, B., Wu, D.Y., Panneerselvam, R. and Tian, Z.Q. (2016) Nanostructure-Based Plasmon-Enhanced Raman Spectroscopy for Surface Analysis of Materials. *Nature Reviews Materials*, **1**, Article No. 16021. https://doi.org/10.1038/natrevmats.2016.21

[21] Wu, D.Y., Li, J.F., Ren, B. and Tian, Z.Q. (2008) Electrochemical Surface-Enhanced Raman Spectroscopy of Nanostructures. *Chemical Society Reviews*, **37**, 1025-1041. https://doi.org/10.1039/b707872m

[22] Olson, T.Y., Schwartzberg, A.M., Liu, J.L. and Zhang, J.Z. (2011) Raman and Surface-Enhanced Raman Detection of Domoic Acid and Saxitoxin. *Applied Spectroscopy*, **65**, 159-164. https://doi.org/10.1366/10-05910

[23] Huai, Q.Y., Gao, C.L., Miao, J.L., Yao, H.L. and Wang, Z.L. (2013) Fast Detection of Saxitoxin Using Laser Tweezers Surface Enhanced Raman Spectroscopy. *Analytical Methods*, **5**, 6870-6873. https://doi.org/10.1039/c3ay41504j

[24] Müller, C., Glamuzina, B., Pozniak, I., Weber, K., Cialla, D., Popp, J. and Cîntă Pînzaru, S. (2014) Amnesic Shellfish Poisoning Biotoxin Detection in Seawater Using Pure or Amino-Functionalized Ag Nanoparticles and SERS. *Talanta*, **130**, 108-115. https://doi.org/10.1016/j.talanta.2014.06.059

[25] Cao, C., Li, P., Liao, H., Wang, J., Tang, X. and Yang, L. (2020) Cys-Functionalized AuNP Substrates for Improved Sensing of the Marine Toxin STX by Dynamic Surface-Enhanced Raman Spectroscopy. *Analytical and Bioanalytical Chemistry*, **412**, 4609-4617. https://doi.org/10.1007/s00216-020-02710-9

[26] Cheng, S., Zheng, B., Yao, D., Wang, Y., Tian, J., Liu, L., Liang, H. and Ding, Y. (2019) Determination of Saxitoxin by Aptamer-Based Surface-Enhanced Raman Scattering. *Analytical Letters*, **52**, 902-918. https://doi.org/10.1080/00032719.2018.1505900

[27] Zhao, P., Liu, H., Zhu, P., Ge, S., Zhang, L., Zhang, Y. and Yu, J. (2021) Multiple Cooperative Amplification Paper SERS Aptasensor Based on AuNPs/3D Succulent-Like Silver for Okadaic Acid Quantization. *Sensors and Actuators B: Chemical*, **344**, Article ID: 130174. https://doi.org/10.1016/j.snb.2021.130174

[28] Lee, P.C. and Meisel, D. (1982) Adsorption and Surface-Enhanced Raman of Dyes on Silver and Gold Sols. *The Journal of Physical Chemistry C*, **86**, 3391-3395. https://doi.org/10.1021/j100214a025

[29] Dendisová-Vyškovská, M., Prokopec, V., Člupek, M. and Matějka, P. (2012) Comparison of SERS Effectiveness of Copper Substrates Prepared by Different Methods: What Are the Values of Enhancement Factors? *Journal of Raman Spectroscopy*, **43**, 181-186. https://doi.org/10.1002/jrs.3022

[30] McFarland, A.D., Young, M.A., Dieringer, J.A. and Van Duyne, R.P. (2005) Wavelength-Scanned Surface-Enhanced Raman Excitation Spectroscopy. *The Journal of Physical Chemistry B*, **109**, 11279-11285. https://doi.org/10.1021/jp050508u

[31] Agnihotri, S., Mukherji, S. and Mukherji, S. (2014) Size-Controlled Silver Nanoparticles Synthesized over the Range 5-100 nm Using the Same Protocol and Their Antibacterial Efficacy. *RSC Advances*, **4**, 3974-3983. https://doi.org/10.1039/C3RA44507K

[32] Bhui, D.K., Bar, H., Sarkar, P., Sahoo, G.P., De, S.P. and Misra, A. (2009) Synthesis and UV—Vis Spectroscopic Study of Silver Nanoparticles in Aqueous SDS Solution. *Journal of Molecular Liquids*, **145**, 33-37. https://doi.org/10.1016/j.molliq.2008.11.014

[33] Yang, L., Hu, J., He, L., Tang, J., Zhou, Y., Li, J. and Ding, K. (2017) One-Pot Synthesis of Multifunctional Magnetic N-Doped Graphene Composite for SERS Detection, Adsorption Separation and Photocatalytic Degradation of Rhodamine 6G. *Chemical Engineering Journal*, **327**, 694-704. https://doi.org/10.1016/j.cej.2017.06.162

[34] Seney, C.S., Gutzman, B.M. and Goddard, R.H. (2009) Correlation of Size and Surface-Enhanced Raman Scattering Activity of Optical and Spectroscopic Properties for Silver Nanoparticles. *The Journal of Physical Chemistry C*, **113**, 74-80. https://doi.org/10.1021/jp805698e

[35] Boca, S.C., Farcau, C. and Astilean, S. (2009) The Study of Raman Enhancement Efficiency as Function of Nanoparticle Size and Shape. *Nuclear Instruments and Methods in Physics Research Section B: Beam Interactions with Materials and Atoms*, **267**, 406-410. https://doi.org/10.1016/j.nimb.2008.10.020

[36] Wang, S., Yan, X., Zhang, M., Dong, G., Moro, R., Ma, Y. and Ma, L. (2022) Real-Time Size Tuning and Measuring of Silver Nanoparticles by Cyclic voltamMetry and Raman Spectroscopy. *Materials Letters*, **310**, Article ID: 131420. https://doi.org/10.1016/j.matlet.2021.131420

[37] Pustovit, V.N. and Shahbazyan, T.V. (2005) Quantum-Size Effects in SERS from Noble-Metal Nanoparticles. *Microelectronics Journal*, **36**, 559-563. https://doi.org/10.1016/j.mejo.2005.02.069

[38] Park, S.G., Mun, C., Xiao, X., Braun, A., Kim, S., Giannini, V., Maier, S.A. and Kim, D.H. (2017) Surface Energy-Controlled SERS Substrates for Molecular Concentration at Plasmonic Nanogaps. *Advanced Functional Materials*, **27**, Article ID: 1703376. https://doi.org/10.1002/adfm.201703376

[39] Jiang, Y., Wang, J., Malfatti, L., Carboni, D., Senes, N. and Innocenzi, P. (2018) Highly Durable Graphene-Mediated Surface Enhanced Raman Scattering (G-SERS) Nanocomposites for Molecular Detection. *Applied Surface Science*, **450**, 451-460. https://doi.org/10.1016/j.apsusc.2018.04.218

[40] Huang, C.C. and Chen, W. (2018) A SERS Method with Attomolar Sensitivity: A Case Study with the Flavonoid Catechin. *Microchimica Acta*, **185**, Article No. 120. https://doi.org/10.1007/s00604-017-2662-9

[41] Medhioub, A., Medhioub, W., Amzil, Z., Sibat, M., Bardouil, M., Ben Neila, I., Mezghani, S., Hamza, A., Lassus, P. (2009) Influence of Environmental Parameters on Karenia Selliformis Toxin Content in Culture. *Cahiers de Biologie Marine*, **50**, 333-342.

[42] Kamal, S. and Yang, T.C.K. (2022) A Novel Ag_2SO_3 Microcrystal Substrate for Highly Sensitive SERS Sensing of Multifold Organic Pollutants. *Journal of Alloys and Compounds*, **898**, Article ID: 162919.

https://doi.org/10.1016/j.jallcom.2021.162919

[43] Kim, J.A., Wales, D.J., Thompson, A.J. and Yang, G.Z. (2020) Fiber-Optic SERS Probes Fabricated Using Two-Photon Polymerization for Rapid Detection of Bacteria. *Advanced Optical Materials*, **8**, Article ID: 1901934. https://doi.org/10.1002/adom.201901934

[44] Cong, S., Wang, Z., Gong, W.B., Chen, Z.G., Lu, W.B., Lombardi, J.R. and Zhao, Z.G. (2019) Electrochromic Semiconductors as Colorimetric SERS Substrates with High Reproducibility and Renewability. *Nature Communications*, **10**, Article No. 678. https://doi.org/10.1038/s41467-019-08656-6

[45] Zhang, P., Gao, J. and Sun, X.H. (2015) An Ultrasensitive, Uniform and Large-Area Surface-Enhanced Raman Scattering Substrate Based on Ag or Ag/Au Nanoparticles Decorated Si Nanocone Arrays. *Applied Physics Letters*, **106**, Article ID: 043103. https://doi.org/10.1063/1.4906800

Supporting Tables and Figures

Table S1. The assignment of main peaks and vibrational mode of gymnodimine.

DFT (cm^{-1})	SERS (cm^{-1})	Band assignment
620	612	υ (C-C), β (CH_2)
820	834	υ (C-O), β (C-C)
1047	1061	υ (C-C), β (-OH)
1298	1301	γ (CH_2)
1416	1407	γ (CH),γ (CH_2) γ (CH_2)
1452	1443	β (CH_2)
1735	-	υ (C=N)

β = in-plane bending vibration; γ = out-of-plane bending vibration; υ = stretching vibration.

Table S2. Experimental conditions and response values for the detection method of GYM

NO.	A The volume of TSC (mL)	B The concentration of Ag NPs (mg/mL)	C DA/Ag NPs ratio	Intensity of GYM (counts)
1	7	5	1	307
2	7	4	2	313
3	7	5	3	145
4	7	6	2	247
5	9	4	3	239
6	9	5	2	681
7	9	5	2	661
8	9	4	1	352
9	9	5	2	680
10	9	6	3	162
11	9	6	1	209
12	9	5	2	653
13	9	5	2	692
14	11	6	2	223
15	11	5	3	104
16	11	5	1	287
17	11	4	2	266

Table S3. Regression equation and R^2 based on characteristic peaks for the quantification of GYM.

	Peak/cm^{-1}	Regression equation	R^2
Methanol solution	1301	y = 29.776x + 30.937	0.9737
	1443	y = 86.224x + 46.771	0.9873
Lake samples	1310	y = 76.474x – 21.899	0.9705
	1447	y = 117.555x + 74.237	0.9913
Shellfish samples	1305	y = 56.771x + 69.342	0.9769
	1445	y = 72.658x + 86.679	0.9897

Table S4. Recovery experiments result of GYM in real samples.

Spiked concentration (μM)	Lake sample		Shellfish sample	
	Detected concentration (μM)	Recovery (%)	Detected concentration (μM)	Recovery (%)
10	9.56 ± 0.51	96	11.62 ± 0.42	116
8	8.30 ± 0.43	104	9.00 ± 0.46	112
6	6.18 ± 0.35	103	6.55 ± 0.27	109
4	4.32 ± 0.38	108	4.49 ± 0.28	112
2	1.86 ± 0.27	93	2.35 ± 0.21	117
1	1.15 ± 0.12	115	0.95 ± 0.10	95
0.5	0.46 ± 0.06	91	0.45 ± 0.07	90

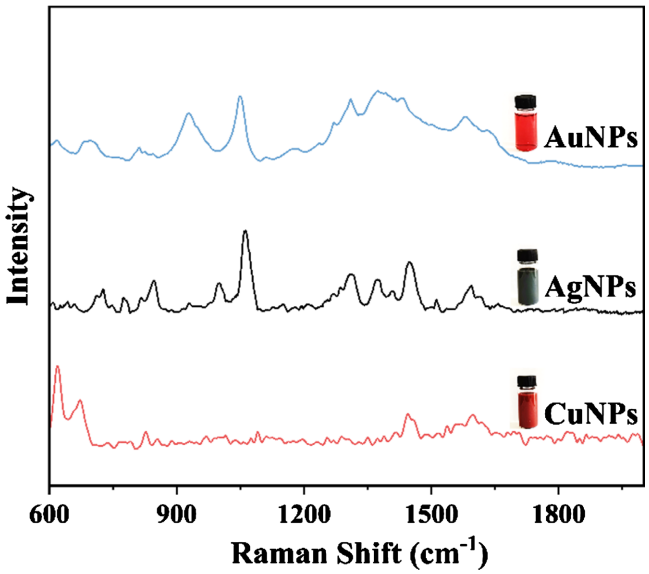

Figure S1. Raman spectra of gymnodimine based on different SERS substrate materials.

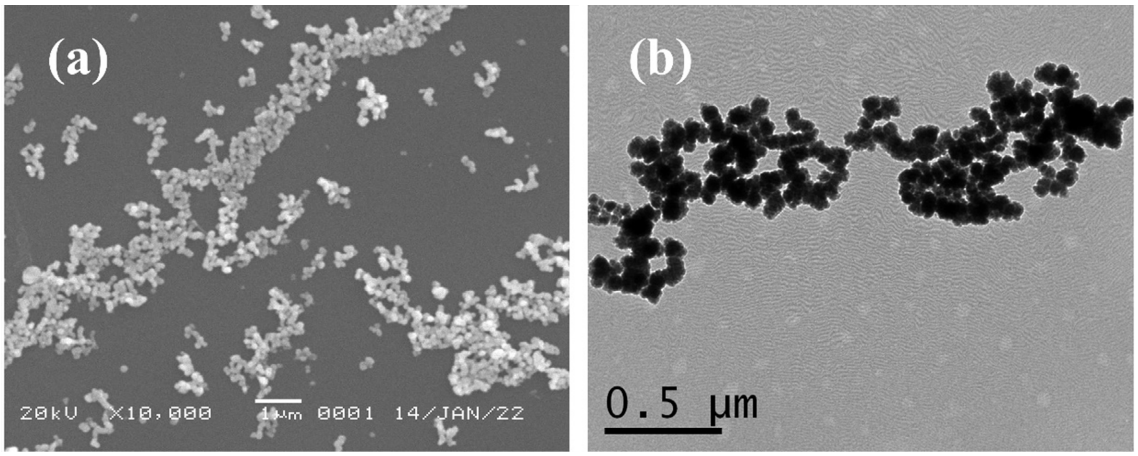

Figure S2. Scanning electron microscopy (a) and transmission electron microscopy (b) images of Silver Nanoparticles (AgNPs).

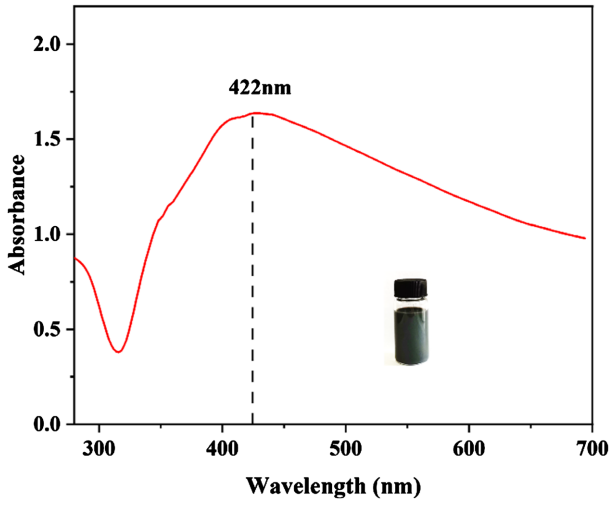

Figure S3. UV-vis absorption spectra of AgNPs.

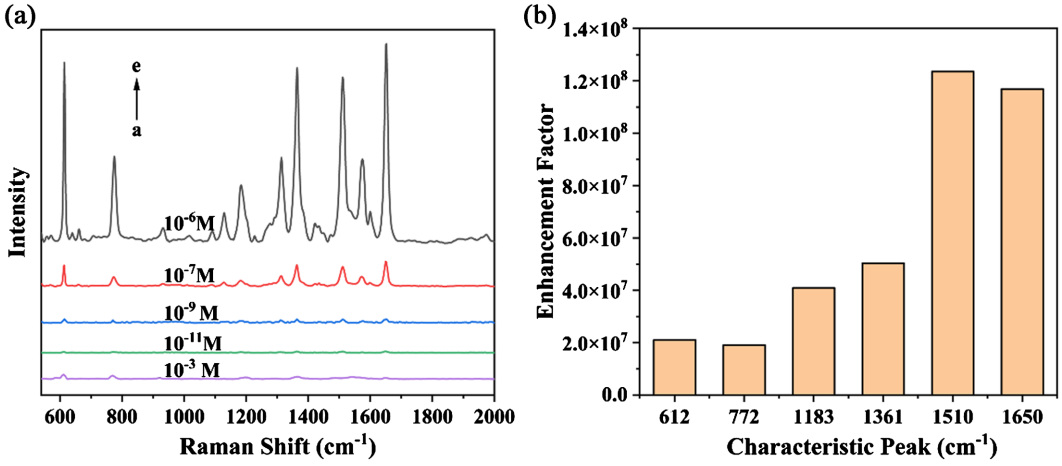

Figure S4. (a) Raman spectra of Rhodamine R6G. (a) Raman spectra of rhodamine R6G solution at 10^{-3} M; SERS spectra of Rhodamine R6G at different concentrations: (b) 10^{-11} M, (c) 10^{-9} M, (d) 10^{-7} M, (e) 10^{-6} M. (b) Enhancement factor (EF) of rhodamine R6G at different characteristic peaks.

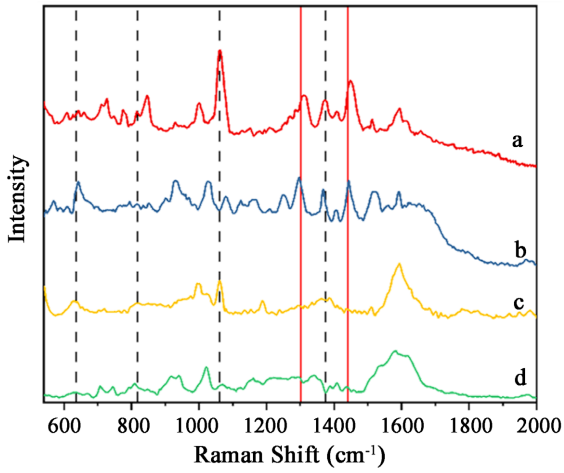

Figure S5. SERS spectra of (a) GYM in lake sample; (b) GYM in shellfish matrix; (c) methanol solution; (d) AgNPs colloidal substrate.